



UPPSALA UNIVERSITET

Analysis of Lohengrin Ionization Chamber Test Run

January 18, 2024

Report for 1FA492 - Project in Applied Physics (15 HP)

Oliver Kraft

oliver.kraft.9720@student.uu.se

Uppsala University

Supervisor:

Ali Al-Adili

ali.al-adili@physics.uu.se

Uppsala University

Contents

| | |
|--|----|
| 1. Introduction | 3 |
| 1.1. Objectives | 4 |
| 1.2. Measurements | 5 |
| 2. Theoretical Background | 5 |
| 2.1. The Fission Process | 5 |
| 2.2. Ions in Matter | 6 |
| 2.2.1. SRIM & TRIM | 6 |
| 3. The Lohengrin Mass-Spectrometer | 6 |
| 3.1. Ionization Chambers | 8 |
| 3.2. The ΔE - E Method | 9 |
| 4. Experimental Setup | 9 |
| 4.1. The Foils | 11 |
| 5. Methodology | 11 |
| 5.1. Gain Correction | 12 |
| 5.2. Curve-Fitting of Spectra | 12 |
| 5.3. Energy Calibration | 13 |
| 5.4. Isotope Identification | 13 |
| 5.5. Resolution Analysis | 14 |
| 6. Results | 14 |
| 6.1. Gain Correction | 14 |
| 6.2. Mass-Energy Identification | 16 |
| 6.3. Isotope Identification | 17 |
| 6.4. Trapezoidal Filter Tuning & Energy Dependence | 19 |
| 6.5. Foil Performance | 21 |
| 7. Discussion | 22 |
| 7.1. Gain Correction Issues | 22 |
| 7.2. Resolution without Foil | 23 |
| 7.3. Isotope Identification | 23 |
| 7.4. Foil Performance | 24 |
| 8. Conclusion & Outlook | 25 |
| Acknowledgements | 25 |
| References | 26 |

Abstract

This project studies the energy resolution and nuclear charge resolution of an ionization chamber (IC) setup connected to the Lohengrin Mass-Spectrometer ahead of a fission yield experiment on Uranium 233. The energy resolution of the IC was found to be $E_{\text{FWHM}} = 640(2)$ keV at $E_{\text{kin}} = 90$ MeV (mass $A = 90$). For isotopic separation, two different foil stacks were tested. The two stacks were found to achieve a worst case nuclear charge resolution of $Z/\Delta Z = 40$ for $Z = 37$ and $Z/\Delta Z = 45$ for $Z = 39$, respectively. However, the poor energy resolution of the second stack makes the first foil a better choice. The achieved nuclear charge resolution with this foil should be sufficient for the lighter masses which are to be studied in the upcoming fission yield experiment.

1. Introduction

Measurements of thermal neutron-induced fission yields of Uranium 233 have been limited compared to other fissioning systems, particularly in the super-asymmetric regime, i.e. when one fission product is very light and one is very heavy. This region, referred to as the “Super-Asymmetric Region” in figure 1, which shows thermal neutron-induced fission yields for ^{233}U . An upcoming experiment performed by a group from Uppsala University aims to rectify this by measuring ^{233}U yields in the super-asymmetric regime. This project analyzes an instrument test performed in preparation of this yield measurement.

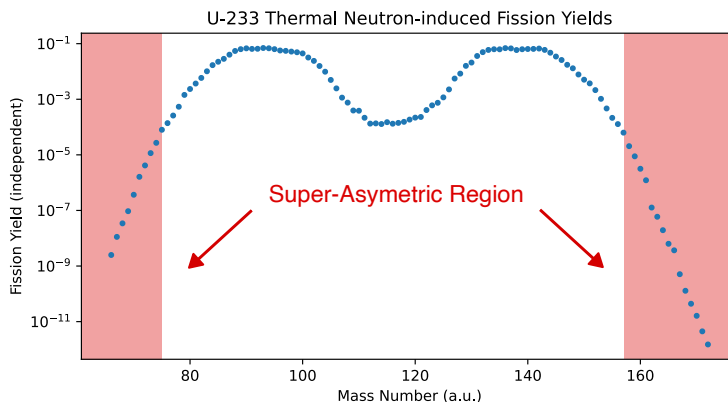


Figure 1: Thermal neutron-induced fission yields post prompt neutron emission as a function of mass-number A for ^{233}U . [1] The super-asymmetric region is also highlighted.

The absence of measurements in the super-asymmetric regime is curious considering the interest in ^{233}U for nuclear technology, and the importance of fission yield data for nuclear physics. For nuclear technology it is of interest due to its role in the thorium fuel cycle. Natural thorium, ^{232}Th , is not itself fissile. However, it is fertile, meaning that it can capture a neutron to form ^{233}U via double beta-decay of ^{233}Th . A nuclear reactor utilizing the thorium fuel cycle would produce energy through the fission of ^{233}U . [2] Understanding the fission products produced is therefore important both for operations and for waste management, should such a reactor be constructed.

From a fundamental physics perspective, the fission process is not yet fully understood, and experimental fission yields are highly useful as benchmarks for fission models. There have been measurements of many other commonly discussed fissioning systems, e.g. ^{235}U [3] and ^{245}Cm [4],

in the super-asymmetric regime. Additional data-points from ^{233}U would be highly valuable for the development of improved fission models, and could give new insights into the fission process.

In particular the thermal neutron-induced fission yields for ^{233}U have never been measured for mass numbers below $A < 80$. The upcoming yield measurement therefore aims to measure isotopic yields, i.e. yields for individual isotopes, from $A = 82$ down to $A \approx 67$, or as low as yields and time will allow. This will allow for overlap with existing results for $A > 80$, and novel measurements for $A < 80$.

The upcoming measurement will take place at Institute Laue-Langevin (ILL) in Grenoble, France. ILL has a specialized instrument for producing fission products called Lohengrin [5] which uses the ILL research reactor to produce ionized fission products. Lohengrin is a mass-spectrometer which can select for fission products based on their mass, ionic charge and kinetic energy (see section 3.). Because of the way Lohengrin does this products can be uniquely identified in terms of their mass simply by measuring the kinetic energy as they exit Lohengrin. This energy will be measured using an ionization chamber (IC) for the upcoming measurement.

To enable identification individual isotopes, i.e. to separate fission products based on their nuclear charge, a foil stack will be inserted between the IC and Lohengrin. As the ionized fission products pass through this foil they will be slowed down differently depending on their nuclear charge. The peaks visible in the energy spectrum without foil will appear “split” after inserting the foil, where the additional peaks correspond to individual nuclear charges. However, this separation comes at the cost of energy resolution, and if the wrong foil is used, the resolution could become so low that nuclear charges cannot be resolved.

This project analyzes an instrument test which was performed to ensure that the intended measurement setup will work for the upcoming measurement. Fission products were measured with and without foil in front of the IC. The idea being to test the performance of both the foils and the IC itself. Two different foil stacks of unknown quality which ILL had on hand were tested, based on this report a decision will be made whether to use one of these or if a new foil stack should be acquired for the yield measurement. The objectives are specified in more detail in section 1.1.

This report is structured as follows; first the underlying physics will be presented in section 2. The instrument used for the measurement, Lohengrin, along with the measurement technique (the ΔE - E method) will then be explained in section 3. The specific measurement setup used in the instrument test will then be presented in section 4. along with the foils in section 4.1. The methodology used in the analysis is described in in section 5. Followed by the results in section 6. The results will then be discussed in section 7. Finally the conclusions from the discussion will be summarized and an outlook will be given in section 8.

1.1. Objectives

The main objective of this project is to investigate two different foil stacks and determine whether either of them would be suitable for the upcoming measurement of ^{233}U . The final measurement aims to measure masses below $A = 80$, where nuclear charges of around $Z = 30$ are expected. The foils thus need to provide sufficient charge separation and energy resolution to enable reliable determination of isotopic yields in this region. The criterion for sufficient in this case will be defined as $\Delta Z/Z > 35$. Essentially this means that neighboring nuclear charges

need to be separated by at least one FWHM (Full Width Half Maximum) for $Z < 35$ in the energy spectrum measured by the ionization chamber.

Additionally, the resolution of the IC itself will be calculated, and any identified procedural issues will be discussed so that they can be addressed ahead of the yield measurement. Of particular interest is the tuning of the trapezoidal filter which is applied to the signal from the ionization chamber.

1.2. Measurements

The measurements for this instrument test were taken at Lohengrin with a Uranium 235 target by Ali Al-Adili (UU), Oliver Kraft (UU), Ulli Koester (ILL) and Jean-Michel Daugas (ILL) in June 2024. For the test two days of beamtime were available. During this the ionization chamber was used without any foils and with each of the two foil stacks installed. Additionally, two different settings on the trapezoidal filter were tested without foil. Lohengrin is described in greater detail in below in section 3. and the measurement setup in section 4.

2. Theoretical Background

This section describes some underlying physics required to understand the report, i.e. what fission is and how ions behave in matter.

2.1. The Fission Process

Fission is the nuclear reaction by which a nucleus splits. The focus of this project is on thermal neutron-induced fission, i.e. when fission is caused by a nucleus capturing a neutron of thermal energy ($E_{\text{kin}} \sim 25 \text{ meV}$). An illustration of the fission process is shown in figure 2 inspired by a similar figure in Lilley [6]. The figure depicts an ^{235}U nucleus capturing a neutron and forming a highly excited ^{236}U compound nucleus. Because of the high excitation this compound nucleus will deform. If the excitation is strong enough this deformation will reach a critical point at which the Coulomb force can overcome the nuclear force keeping the nucleus together. The nucleus then splits in two, with the two fragments gaining a large amount of kinetic energy from the Coulomb potential which drives them apart. Simultaneously, a number of prompt neutrons are emitted alongside gamma rays. [6]

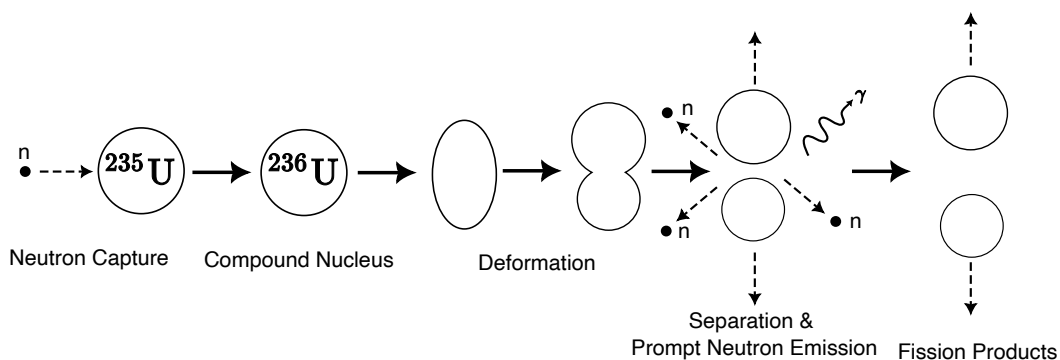


Figure 2: Illustration of the fission process from neutron capture to formation of fission products. Inspired by similar figure in [6]

Around 200 MeV is released in the fission process, with about 90% going into the kinetic energy of the fission products. Typically one lighter and one heavier product is produced, as

is illustrated in figure 1. The energy is distributed between the fission products according to momentum conservation, the lighter product therefore receives higher kinetic energy than the heavier product. [6]

2.2. Ions in Matter

Fission products produced by Lohengrin are typically highly ionized. [7] This ionization is important because ions lose energy as they pass through matter, primarily through Coulombic interaction and, to a lesser extent via collisions. The rate of energy loss, often called the stopping power dE/dx , is dependent on many different factors, most importantly for this report is the nuclear charge Z and the kinetic energy of the ions. The stopping power increases with Z , and increases with decreasing energy until a threshold is reached after which it falls off. [6] This is utilized in the $\Delta E - E$ method (section 3.2.) to differentiate fission products from Lohengrin by nuclear charge.

There is some amount of variation in both the path taken by the ions through the material and the amount of energy lost per interaction. Because of this, there is some variation in the energy ions lose as they pass through some material. Some ions lose more energy and some lose less, introducing a distribution in energy or broadening a preexisting distribution. This phenomenon is called straggling. [6]

2.2.1. SRIM & TRIM

To compute the energy losses and straggling as ions traverse matter typically numerical simulation tools are used. SRIM (Stopping Range of Ions in Matter) and TRIM (TRansport of Ions in Matter) [8] are examples of such tools. SRIM can produce estimated stopping ranges and stopping powers of ions in a broad range of materials using advanced empirical models based on measurements. TRIM is a Monte Carlo based simulation tool which simulates the motion of ions through matter, and enables the extraction of many different parameters including the energy loss.

3. The Lohengrin Mass-Spectrometer

ILL's Lohengrin instrument is a recoil mass-spectrometer built for studying exotic nuclei produced during fission and the fission process itself. It can with very high precision filter out fission products based on their mass, charge and energy. [5] An illustration of the instrument can be seen in figure 3. The figure shows the key components of Lohengrin including the fission target next to the reactor core, the horizontal and vertical deflectors and the refocusing magnet.

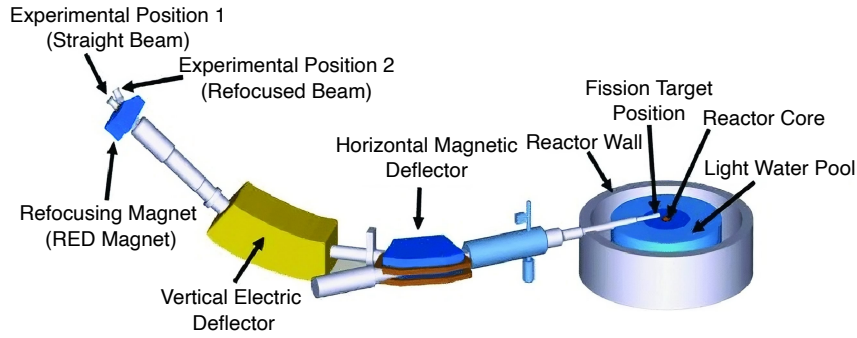


Figure 3: Illustration of Lohengrin highlighting the, source (fission target), horizontal magnetic deflector, vertical electric deflector and refocusing magnet. Illustration from [9] modified with nomenclature from [5]

The fission products for Lohengrin are produced by using a thin film sample made of a fissile actinide. This film is inserted very close to the core of the ILL High-Flux reactor where the sample will undergo fission. At the position of the sample the neutron flux is thermal with a flux of $5 \cdot 10^{14} \text{ cm}^{-2}\text{s}^{-1}$. This high flux leads to a very high rate of fission and enables a wide range of experiments. [10] Most interesting for the upcoming yield measurements is that this high fission rate gives access to very low yield fission products.

When fission occurs in the sample film the products have a very high kinetic energy. Traversing the actinide film at this high energy strips off electrons, ionizing the fission products. These ionized fission products then enter Lohengrin. In Lohengrin they are typically measured at ionic charge states ranging approximately from $Q = 15$ up to $Q = 25$, with a slight dependence on the mass of the product. [7] This ionic charge is key as it enables electromagnetic separation of the products.

Products are selected for based on the mass-charge ratio A/Q and kinetic energy-charge ratio E/Q . The first step is A/Q separation which is performed using the horizontal magnetic deflector. Using a strong magnetic field adjusted to only allow the selected ratio through, the deflector redirects other ratios into the wall of the separator. This is followed by the vertical electric deflector which works similarly, but instead uses a strong electric field to select products of a single E/Q ratio. The result after these two steps is a beam consisting of a single A/Q and E/Q . [5]

The settings on the magnetic and electric field are specified in as $A/E/Q$, from which both the A/Q and E/Q ratios selected for can be read. Note this does not imply that only products with the specified values of A , E and Q are allowed, it is still the ratios A/Q and E/Q that dictate which products are selected for. These ratios can often be achieved by multiple different products. For instance $100/20/100$ does not only produce products corresponding to $A = E = 100$ at a charge state of $Q = 20$. All other fission products corresponding to $A/Q = E/Q = 5$ are also produced, e.g. $A = E = 90$ at a charge state of $Q = 18$.

Attached to the output is a refocusing magnet, the RED magnet. This magnet can be optionally used reduce the spot size of the beam, enabling higher intensities and count rates for experiments. [10] The RED magnet redirects the beam, when it is in use the detector setup needs

to placed at “Experimental Position 2”, as seen in figure 3. If the RED magnet is not active “Experimental Position 1” is used, where the beam passes straight from Lohengrin.

3.1. Ionization Chambers

Because multiple different products could have the same A/Q and E/Q ratio, an additional component is required to identify individual products. For this purpose, an ionization chamber can be utilized to measure the energy. An ionization chamber is a chamber filled with a gas, an ion flying through the gas will ionize it, freeing electrons and losing energy in the process. By applying an electric field over the chamber these freed electrons can be captured and measured. The number of electrons is equal to the number of ionization events in the IC gas, which will be proportional to the kinetic energy of the ions. [11]

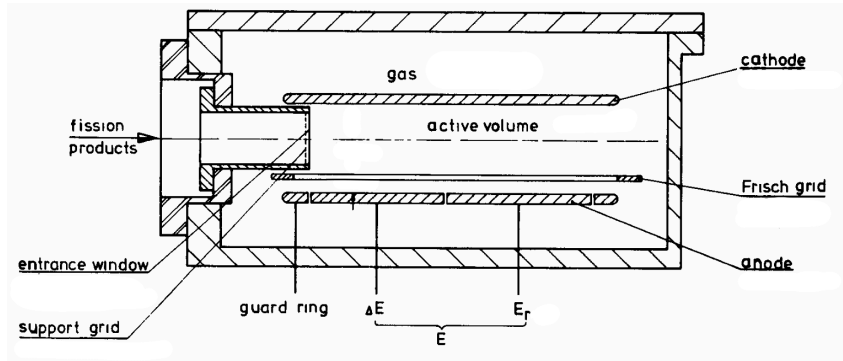


Figure 4: A schematic of an ionization chamber with labeled components. [12]

A schematic of an ionization chamber similar to the one used here can be seen in figure 4. Shown in the figure is the pressure chamber enclosing the key components of the IC. Inside the chamber the anode and cathode are highlighted. Note here that the anode is split into two segments, ΔE and E_r . These two segments are separated by a separation grid which is set to a ground potential. This makes it possible to independently measure the energy deposited in each of the two regions independently. As the chamber is filled with a gas but the Lohengrin beamline needs to be at vacuum to not disturb the fission products an entrance window is installed. The final important component in the figure is the Frisch-grid. This is a grid electrode which is set to an intermediate potential and used to cancel the drift-time of the electrons in the chamber. [11]

The kinetic energy measurements with an IC connected to Lohengrin are typically presented as a 1D histogram, a spectrum. Each spectrum will contain a sum of Gaussian-shaped peaks:

$$f(E) = \sum_i A_i \exp\left(-\frac{(E - \mu_i)^2}{2\sigma_i^2}\right) \quad (1)$$

where E is the kinetic energy and the peaks are indexed by i . The parameter A_i is the height, σ_i is the standard deviation, and μ_i is the centroid of peak i .

To simplify the discussion later it is useful to view each peak in a spectrum as the sum of a series of normally distributed random variables. The variance for the major contributors are:

- σ_{noise}^2 : Variance of measurement noise.
- $\sigma_{\text{statistical}}^2$: Variance of statistical uncertainty, arising due to the finite number of counts.

- $\sigma_{\text{instrument}}^2$: Variance of the energy distribution produced by Lohengrin, as well as straggling in the IC gas and the fission target film. Slightly dependent on kinetic energy.

The total variance for an individual peak in the energy spectrum can then be described as:

$$\sigma_{\text{total}}^2 = \sigma_{\text{noise}}^2 + \sigma_{\text{statistical}}^2 + \sigma_{\text{instrument}}^2 \quad (2)$$

3.2. The ΔE - E Method

The way Lohengrin separates products makes it possible to unambiguously identify products by mass by simply measuring the energy, for instance using an ionization chamber. However, to distinguish different nuclear charges (Z) another step is required. A commonly used method for this is the so called ΔE - E method. In section 2.2. it was mentioned that stopping power increases with nuclear charge. This can be utilized to create an energy separation between nuclear charges by adding an absorber in front of the IC. The absorber will cause peaks in the energy spectrum previously corresponding to masses to split into subpeaks corresponding to individual nuclear charges. Lower energy subpeaks represent higher nuclear charges as these lose more energy in the absorber, and vice versa for higher energy subpeaks. [11]

One way to realize this is to use an IC split into two segments, as the IC used here is. The ΔE segment could function as a gaseous absorber whilst simultaneously measuring the energy loss. This generally gives lower nuclear charge resolution than the other alternative, solid absorbers. These are typically a few micrometers of foil which is inserted in front of the energy detector. When using a solid absorber alongside a split IC typically the segments in the chamber are summed, so that only the total energy is measured. [12]

When an absorber is inserted in front of the IC an additional normally distributed random variable can be added to the description presented in section 3.1. Equation (2) can then be expanded to:

$$\sigma_{\text{total}}^2 = \sigma_{\text{noise}}^2 + \sigma_{\text{statistical}}^2 + \sigma_{\text{instrument}}^2 + \sigma_{\text{absorber}}^2 \quad (3)$$

where the additional term $\sigma_{\text{absorber}}^2$ represents the variance from straggling in the absorber. In the case of solid absorbers, foils, imperfections from manufacturing or damage are also included in this term. This equation will be useful when discussing the energy resolution and nuclear charge separation as there is a trade-off between these two characteristics. A thicker absorber provides greater separation as separation is directly related to the energy loss in the absorber. However, a thicker absorber also leads to increased broadening due to straggling, and potentially a larger risk of imperfections. [13]

4. Experimental Setup

The measurements were performed with an ^{235}U sample installed in Lohengrin. This is a different isotope than will be used in the yield measurement this spring. However, because the goal of the test is to measure resolution and not yields this does not matter. The detector setup with the ionization chamber and foil mount can be seen in figure 5. The figure shows the IC attached to a T-shaped beampipe with the foil mount, this is then mounted to “Experimental Position 1” from figure 3. The RED magnet was not used during this test measurement.

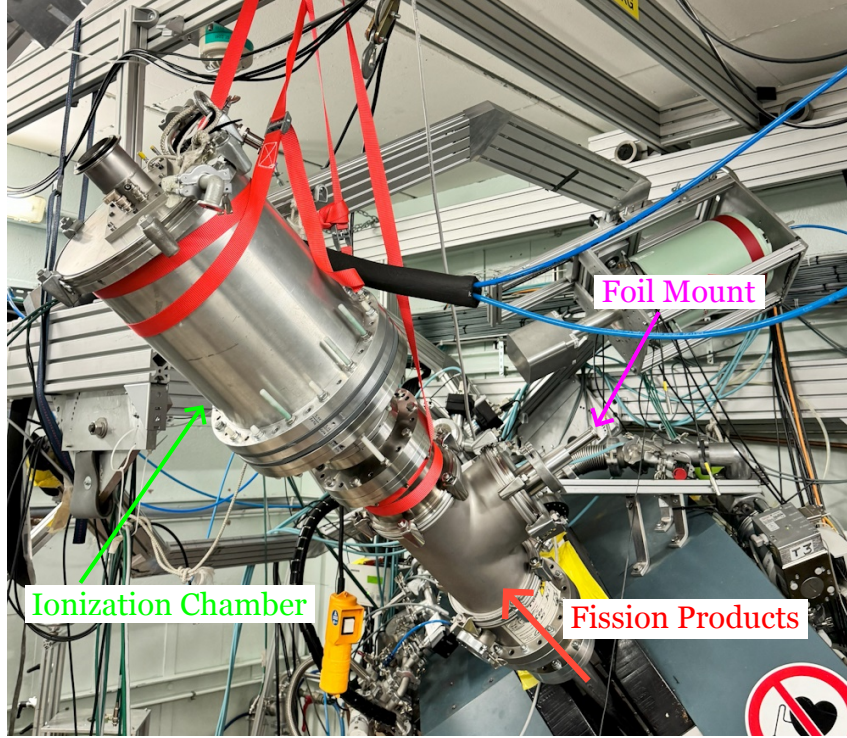


Figure 5: An annotated image of the measurement setup. Highlighted is the ionization chamber, the foil mount in a T-shaped beampipe and the direction of the fission products.

The IC used here was very similar to the one shown in figure 4, i.e. a two segment Frisch-grid IC. For these measurements the entrance window used was a 2000 Å thick layer of Silicon Nitride, and the chamber was filled with isobutane at 40 mbar. Both anodes were set to a potential of +800 V and the Frisch Grid was set to +400 V, which was high enough to cancel the drift time whilst avoiding electrical arcs in the chamber.

Each section of the two-segment ionization chamber was connected to its own preamplifier. These preamplifiers were then connected to an analogue to digital converter (ADC) and a trapezoidal filter was applied. The trapezoidal filter converts the pulses from the preamplifiers into trapezoidal-shaped pulses. These provide a reliable way of measuring the intensity of the pulses as the area of the trapezoids. Computing the area involves integrating over multiple time-steps leading to a cancellation of many minor disturbances.

The trapezoidal filter has the following parameters to adjust its output:

- The gain G which adjusts the height of the trapezoid.
- The rise time T_{rise} , the time to reach the top of the trapezoid.
- The decay time T_{decay} , the time for the trapezoid to decay to zero.
- The peak delay τ_{delay} , is the time from the end of the rise until the decay starts.

The performed measurements have been divided into three series based on the settings used for these parameters. Table 1 shows these settings. The first series, taken without foil and denoted as *no_foil_1* was chronologically the first to be performed. In an attempt to improve the energy resolution seen in the live-view whilst measuring the settings were adjusted for *no_foil_2*. After adding the foils an additional small adjustment was made to T_{rise} .

Table 1: The table different measurement series alongside the trapezoidal filter settings used for the trapezoidal filter connected to each of the two segments of the Ionization Chamber (ΔE and E_r). Specifically, the gain G , rise time T_{rise} , decay time T_{decay} and the peak delay τ_{delay} are listed.

| Series | Segment | T_{rise} (μs) | G | T_{decay} (μs) | τ_{delay} (μs) |
|-----------|------------|-------------------------------------|-------|--------------------------------------|---|
| no_foil_1 | ΔE | 4 | 1.5 | 50 | 2 |
| no_foil_1 | E_r | 2 | 5.916 | 48 | 2 |
| no_foil_2 | ΔE | 4 | 2 | 50 | 2 |
| no_foil_2 | E_r | 2 | 2 | 48 | 3 |
| foil | ΔE | 8 | 2 | 50 | 2 |
| foil | E_r | 8 | 2 | 48 | 3 |

4.1. The Foils

The two foil stacks used can be seen in figures 6 and 7. Both foils were most likely made of the polymer Parylene C. Unfortunately, the thickness of these foils is not known. However it is likely around 10 micrometers, based on SRIM data for Polypropylene, a similar polymer. These foil stacks were mounted to an adjustable holder which was adjustable along two axes, it could be moved transversely to the beam direction and it could be rotated. For both foils this position was adjusted to maximize the count rate, which indicates good alignment. Tape was used to block the gaps visible above and below the first foil, preventing fission products from reaching the IC without passing through the foil.

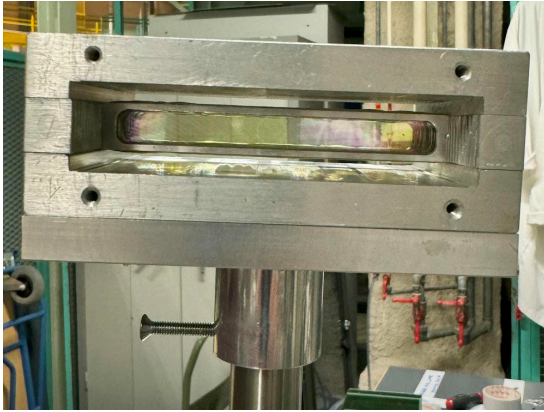


Figure 6: An image of foil 1.



Figure 7: An image of foil 2.

5. Methodology

This section describes the steps taken to post-process and analyze the data obtained from the measurements. Additionally, the metrics used to quantify the resolution of the measurement setup are presented. Below is an overview of the steps taken.

1. Perform a gain correction such that the amplification applied to the signal from both segments of the ionization chamber is the same (section 5.1.).
2. Fit a sum of Gaussian functions to each of the measured spectra (section 5.2.).
3. Identify masses and energies for the measurements without foil to perform an energy calibration (section 5.3.).

4. Identify nuclear charges after adding the foils. (section 5.4.).
5. Use fit and identification results to perform resolution comparison. (section 5.5.).

5.1. Gain Correction

Two separate preamplifiers were used, one for each segment in the ionization chamber. These preamplifiers differed slightly in their internal gain. To obtain the total kinetic energy of the products by adding the signals from the ΔE and E_r segments of the IC, this needs to be corrected for. Typically, this is done at the time of measurement by tuning the gain of the trapezoidal filter. However, because of the limited time available for these measurements it was decided it would be better to perform this correction during the post processing.

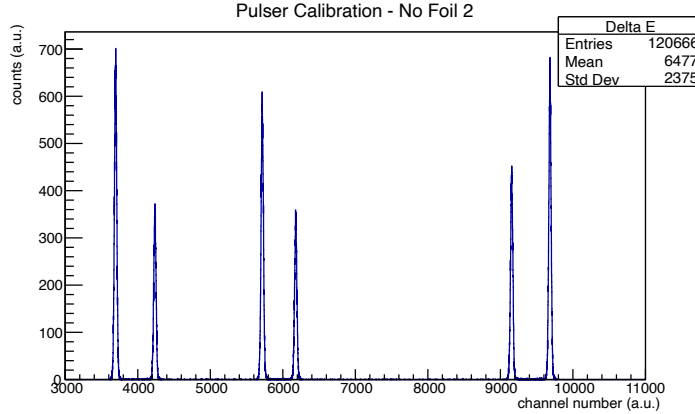


Figure 8: An example measurement from the signal generator.

To enable determination of the relative gain between the two preamplifiers the same signal needs to be sent through both preamplifiers, so that the ratio between their gains can be identified. For this purpose a “synthetic” measurement was taken for each set of settings on the trapezoidal filter. These were produced by connecting a pulse generator to both preamplifiers at the same time. Recording an energy spectrum then produced a synthetic peak, where the “energy” is related to the amplitude of the pulse produced by the pulse generator.

To obtain a more reliable estimate of the difference in amplitude the amplitude of the pulse generator was adjusted whilst recording. This produces synthetic spectra which look something like figure 8, where each peak can be used as a point of comparison between the two preamplifiers. Performing a curve fit with a sum of Gaussian functions makes it possible to obtain the peak positions. Using the positions obtained it is then possible to perform a linear fit between the recorded peak positions from the ΔE and E_r preamplifiers. The gain ratio $G_{\Delta E}/G_{E_r}$ is simply the proportionality constant obtained from this linear fit.

To validate the identified difference gain ratio ΔE - E histograms from a measurement can be utilized. These are 2D histograms with ΔE on the y-axis and total kinetic energy on the x-axis. When the gains are correctly adjusted the individual spots (corresponding to fission products) in this histogram should look circular or elliptical without any inclination or slant. When there is a difference in gain between the two preamplifiers the individual spots will appear slanted.

5.2. Curve-Fitting of Spectra

Curve fitting on the measured spectra was done using CERN’s data analysis framework ROOT. [14] For the measurements taken without foil in front of the ionization chamber a fully correct

treatment was possible, i.e. fitting a sum of Gaussian functions, equation (1), to the measured spectrum. This accounts for the variation in width due to varying numbers of counts and kinetic energy between different masses in the same spectrum.

Ideally, the procedure would have been the same for the measurements with foil, however, due to a combination of the limited energy separation between neighboring nuclear charges of the same mass and the resolution this was not possible. Too many peaks were merged to produce physical fits this way. Instead a constraint was added to the widths of the Gaussians requiring that they all have the same width. Because of the very small difference in energy between neighboring nuclear charges of the same mass this should have a relatively minor effect on the resolution comparisons. Instead of equation (1) the following function was used for the curve fit:

$$f(E) = \sum_i A_i \exp\left(-\frac{(E - \mu_i)^2}{2\sigma^2}\right) \quad (4)$$

Where the only difference is that the standard deviation σ is now the same for all peaks included in the fit.

5.3. Energy Calibration

A calibration needs to be performed to relate channel numbers from the analog to digital conversion performed by the measurement system to the kinetic energy of the incident fission products. This was done separately for the two measurement series recorded without foil, because they used very different settings on the trapezoidal filter. To do this for the measurements with foil the calibration for *no_foil_2* was used, as its settings on the trapezoidal filter were almost identical.

The first step was to identify the allowed energies by the settings used for Lohengrin in each run. The procedure for this involves using an internal ILL spreadsheet which produces a list of candidate products which could reach the IC. These candidates are specified in terms of their mass, charge and incident energy. Relating this to each energy spectrum it is possible to identify each peak by comparing the relative energy of the peaks and the peaks which should be produced by Lohengrin.

The incident energy identified is however not the energy measured by the IC but the energy produced by Lohengrin. The entrance window of the IC reduces the energy of the products somewhat (by ~ 2.5 MeV). This was corrected for by using TRIM to estimate the energy loss in the window. The highest yield nuclear charge based on the yields provided by JAEA [1] for each mass number was taken as an approximation for all fission products with the same mass number. This is not entirely accurate, but the window is thin enough that it is a decent approximation, the difference in energy loss between neighboring nuclear charges is very small in the entrance window.

5.4. Isotope Identification

When the foil is inserted individual isotopes can be identified according to the ΔE - E method. Section 3.2. describes how inserting a foil introduces an additional separation by decelerating fission products differently depending on their nuclear charge. The difference in kinetic energy between neighboring nuclear charges is quite small, a few MeV at most, but provided sufficient resolution should make it possible to discern nuclear charges.

Based on the relative energy of the peaks in a spectrum with foil it is possible to identify the mass for each set of subpeaks by comparing to measurements without foil using the same settings on Lohengrin. To identify isotopes the relative height of each peak was compared to the isotopic yields for that mass number (A) of ^{235}U as taken from JAEA [1], the identification was made be closest match. This is only indicative however, as the fission products are distributed over various charge states and kinetic energies. If the identification is correct the nuclei with higher nuclear charge, and therefore stopping power, should be measured at lower energies by the IC as they lose more energy in the foil.

5.5. Resolution Analysis

Using the energy calibration, the isotope identification and the widths and positions from the curve-fits, the energy resolution of the setup can be analyzed. For this purpose a couple of different metrics will be used. One useful metric for the energy resolution is E_{FWHM}/E , i.e. the full width half maximum divided by the energy. The standard error propagation formula [15]:

$$u(y) = \sqrt{\sum_{i=0} \left(\frac{\partial y}{\partial x_i} \right)^2 u(x_i)^2} \quad (5)$$

can be used for computing the uncertainty $u(y)$ in a quantity $y(x_i)$ based on the uncertainty in its parameters x_i . Applying this to the resolution metric above gives equation (6). In this case the error in the parameters $u(E)$ and $u(E_{\text{FWHM}})$ is given by the fit uncertainty.

$$u\left(\frac{E_{\text{FWHM}}}{E}\right) = \frac{1}{E} \sqrt{u(E_{\text{FWHM}})^2 + \frac{E_{\text{FWHM}}^2}{E^2} u(E)^2} \quad (6)$$

To evaluate if the criterion set for the foil performance, i.e. separation by at least one FWHM for $Z < 35$, the most useful metric is $Z/\Delta Z$. This metric gives an estimate of the highest nuclear charge which will be separated by one FWHM. It is based on a comparison between two neighboring nuclear charges and computed using the following formula:

$$\frac{Z}{\Delta Z} = Z \frac{\delta E}{E_{\text{FWHM}}} \quad (7)$$

Where δE is the difference in energy between neighboring nuclear charges and E_{FWHM} is the Full Width at Half Maximum. The Z referred to in the formula is the nuclear charge of nuclide with the highest kinetic energy out of the two compared. Typically this is rounded down to the nearest integer, as nuclear charges are integers. Because of this rounding it makes little sense to compute the error of this metric. However, for the intermediate expression $\delta E/E_{\text{FWHM}}$ on the other hand the the standard error propagation formula, equation (5), can be applied:

$$u\left(\frac{\delta E}{E_{\text{FWHM}}}\right) = \frac{1}{E_{\text{FWHM}}} \sqrt{u(\delta E)^2 + \frac{(\delta E)^2}{E_{\text{FWHM}}^2} u(E_{\text{FWHM}})^2} \quad (8)$$

6. Results

6.1. Gain Correction

From the synthetic spectra measured using the pulse generator it was possible to determine the difference in gain between the two preamplifiers. The ratio $G_{\Delta E}/G_{E_r}$ was used to quantify this

and is shown in table 2. From the table *no_foil_1* appears to have had the largest difference in gain between the preamplifiers. It also appears that *no_foil_2* and the foils had a very similar difference in gain.

Table 2: The difference in gain for the two different segments as identified using the pulser data.

| Series | $G_{\Delta E}/G_{E_r}$ |
|-----------|------------------------|
| no_foil_1 | 4.8614(3) |
| no_foil_2 | 1.217(3) |
| foils | 1.244(1) |

As described in section 5.1., the gain correction can be validated using ΔE - E histograms. Examples of these are visible in figure 9 for *no_foil_1*, in 10 for *no_foil_2* and in 11 for foil 1, with each subfigure a and b corresponding to before and after gain correction.

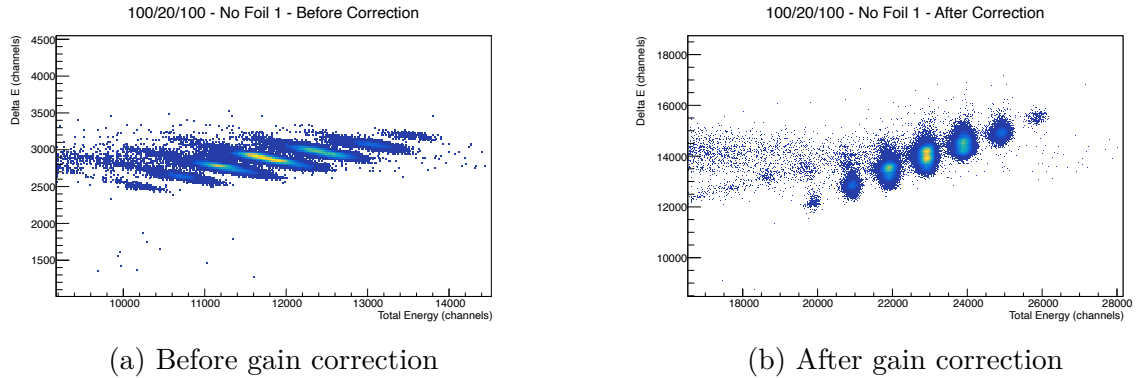


Figure 9: ΔE - E histogram of a measurement taken with Lohengrin set to $A/Q/E = 100/20/100$ before (a) and after (b) performing gain correction for *no_foil_1*.

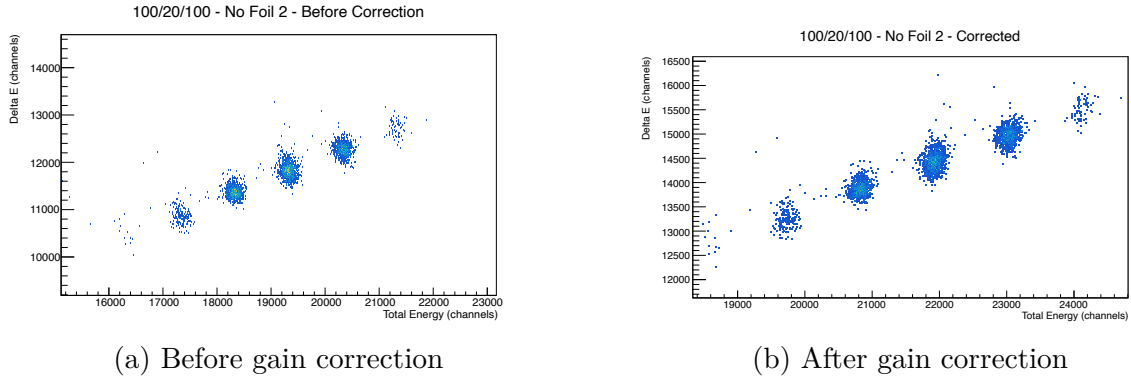
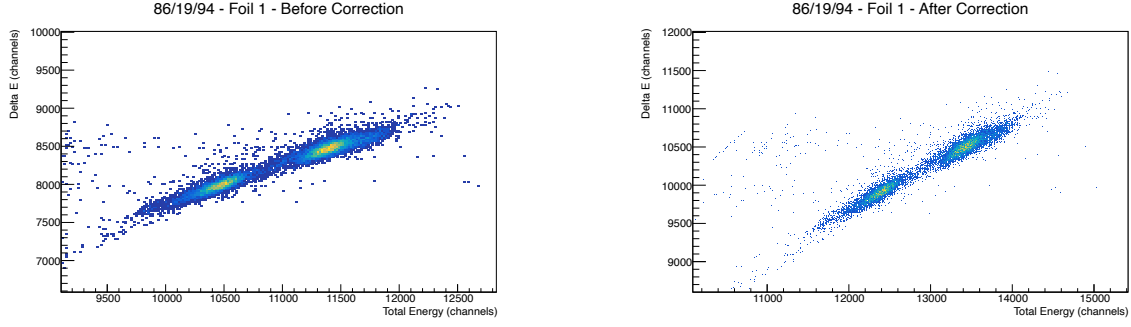


Figure 10: ΔE - E histogram of a measurement taken with Lohengrin set to $A/Q/E = 100/20/100$ before (a) and after (b) performing gain correction for *no_foil_2*.



(a) Before gain correction

(b) After gain correction

Figure 11: ΔE - E histogram of a measurement taken with Lohengrin set to $A/Q/E = 100/20/100$ before (a) and after (b) performing gain correction with foil 1.

This correction worked very well for *no_foil_1*. The severe slant visible in figure 9a disappears completely after correction as can be seen in figure 9b. The other series without foil, *no_foil_2*, requires little correction, though a small reduction in slant is seen in figure 10b compared to figure 10a. However, for the measurements with foil this worked less well. The spots are strongly slanted to begin with here, and in the opposite direction compared to *no_foil_1* as can be seen in figure 11a. After correction a strong slant remains as can be seen in figure 11b. Foil 2 demonstrates the same behavior, only a ΔE - E histogram for foil 1 is therefore shown as an example.

6.2. Mass-Energy Identification

Using the fit-result along with the procedure described in section 5.3., a number of mass-energy pairs could be identified in the measurements without foil. These pairs without energy losses have been highlighted in figure 12 on top of the mass-energy histogram for thermal neutron-induced fission of ^{235}U . The histogram was based on calculations from the GEF (“GEneral description of Fission observables”) [16] fission model code performed by Ali Al-Adili.

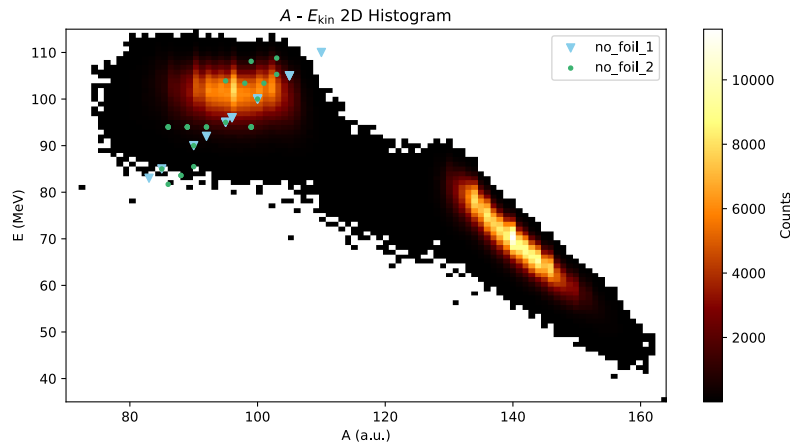


Figure 12: The figure shows a 2D histogram of A and E_{kin} with the mass-energy pairs identified from the measurements without foil overlaid on top. The histogram data is from GEF [16] for the $^{235}\text{U}(n_{\text{th}}, f)$ reaction.

6.3. Isotope Identification

There were multiple examples for both foils which demonstrated separation of peaks corresponding to masses into multiple nuclear charges. One particularly interesting example with foil 1 was visible using the settings $A/Q/E = 92/20/94$ on Lohengrin (notation explained in section 3.). This spectrum can be seen in figure 13, without foil in figure 13a and with foil in 13b. In the figures the blue line is the measured energy spectrum (1D histogram) and the red line is the curve fit. The energy and height identified from the curve fit alongside yields from JAEA [1] are visible in table 3.

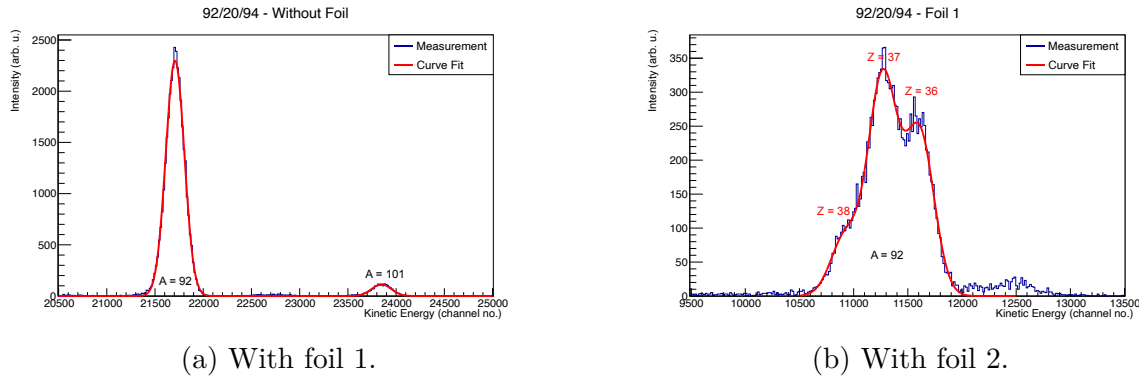
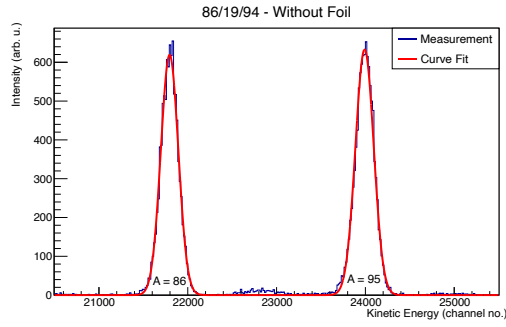


Figure 13: Energy spectra without foil (a) and with foil 1 (b) measured with Lohengrin set to $A/Q/E = 92/20/94$. The plots show both the measured spectrum (blue) and the gaussian curve-fit (red). The masses $A = 92$ and $A = 101$ are visible without foil, the foil causes separation of the $A = 92$ peak into $Z = 38$, $Z = 37$ and $Z = 36$.

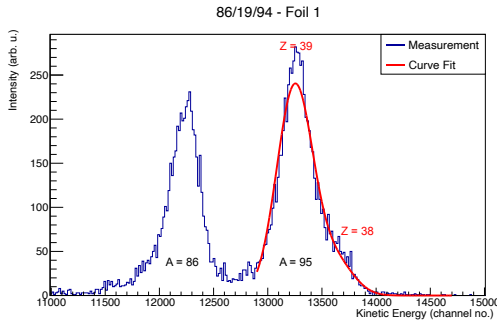
Table 3: A table of the kinetic energy and heights from discernible subpeaks to $A = 92$ in the measurement with foil 1 at $A/Q/E = 92/20/94$ alongside absolute and relative yields for the identified isotopes from [1]. The peaks corresponding to these nuclear charges (Z) are highlighted in figure 13b.

| Peak | 1 | 2 | 3 |
|------------------------|------------------|------------------|------------------|
| E_{kin} (MeV) | 47.0(6) | 48.5(6) | 50.0(6) |
| Height (a.u.) | 64(3) | 237.4(5) | 177.1(6) |
| Nuclide | ^{92}Sr | ^{92}Rb | ^{92}Kr |
| Z | 38 | 37 | 36 |
| Yield (abs.) | 0.93% | 3.35% | 1.65% |
| Yield (rel.) | 0.28 | 1.00 | 0.49 |

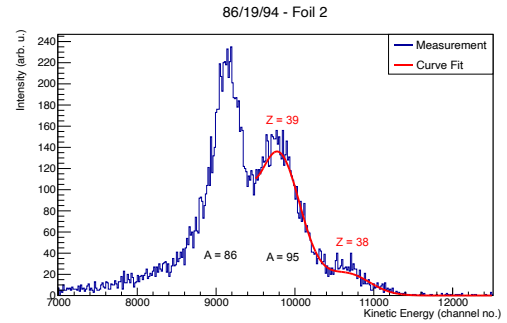
Setting Lohengrin to $86/19/94$ showed splitting with both foils, as can be seen in figure 14. Two different masses are visible in this spectrum, $A = 86$ and $A = 95$, as can be seen in figure 14a taken without foil. With foil 1 (fig. 14b) it appears the higher mass $A = 95$ peak separates ever so slightly and it is possible to fit two peaks corresponding to $Z = 39$ and $Z = 38$. With foil 2 (fig. 14c) the separation appears greater, however the peaks corresponding to the two different masses are almost merged.



(a) Without foil.



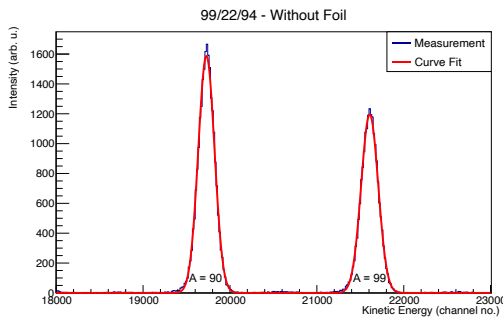
(b) With foil 1.



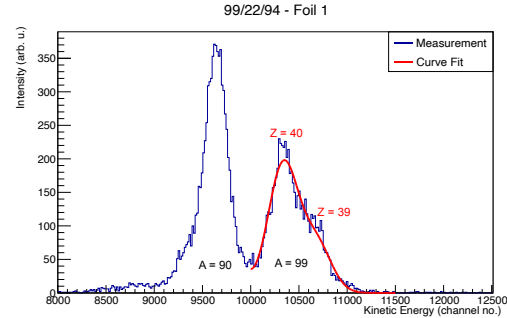
(c) With foil 2.

Figure 14: Energy spectra measured with Lohengrin set to $A/Q/E = 86/19/94$ showing the measured spectrum (blue) and the gaussian curve-fit (red). The masses $A = 86$ and $A = 95$ are visible without foil (a), foil 1 (b) and foil 2 (c) cause separation of the $A = 95$ peak into $Z = 39$ and $Z = 38$.

Another example of a fit with foil 1 can be seen with Lohengrin set to $99/22/94$, this yields figure 15a without and 15b with foil. The figure shows some signs of separation for the lower mass $A = 90$, but it was not possible to fit two peaks to it. The higher mass peak, $A = 99$, shows quite clear separation into $Z = 40$ and $Z = 39$.



(a) Without foil.



(b) With foil 1.

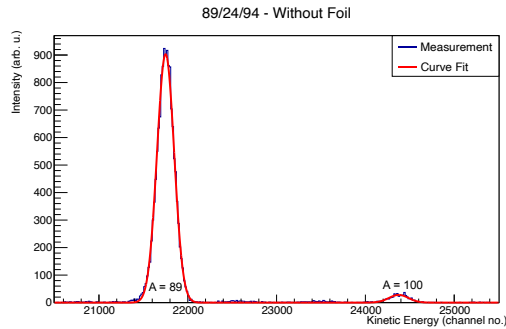
Figure 15: Energy spectra without foil (a) and with foil 1 (b) measured with Lohengrin set to $A/Q/E = 99/22/94$. The plots show both the measured spectrum (blue) and the Gaussian curve-fit (red). The masses $A = 90$ and $A = 99$ are visible, the foil causes separation of the $A = 99$ peak into $Z = 40$, and $Z = 39$.

Another example for foil 2 is found with Lohengrin set to $89/24/94$ shown in figure 16c, with the corresponding measurement without foil in figure 16a. There is clear separation of nuclear charges with foil 2 and one can identify peaks corresponding to Bromine and Krypton ($Z = 35$

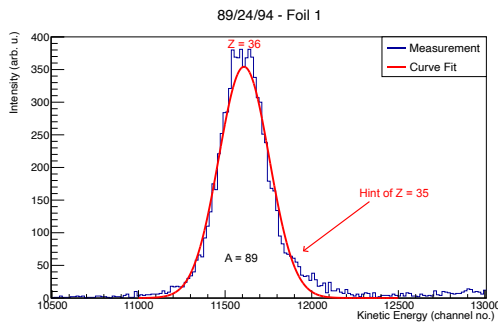
and $Z = 36$). In table 4 the kinetic energies, peak heights and yields can be seen. As a point of comparison figure 16b shows the same settings using foil 1, it was not possible to fit both peaks here however there is a hint of the $Z = 35$ peak.

Table 4: A table of the kinetic energy and heights from discernible subpeaks to $A = 89$ in the measurement with foil 2 at 89/24/94 alongside absolute and relative yields for the identified isotopes from [1]. The peaks corresponding to these nuclear charges (Z) are highlighted in figure 16c.

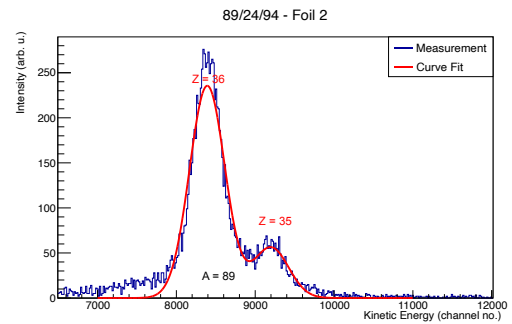
| Peak | 1 | 2 |
|------------------------|------------------|------------------|
| E_{kin} (MeV) | 36(1) | 39(1) |
| Height (a.u.) | 174(3) | 41(1) |
| Nuclide | ^{89}Kr | ^{89}Br |
| Z | 39 | 38 |
| Yield (abs.) | 3.28 % | 1.22 % |
| Yield (rel.) | 1.00 | 0.37 |



(a) Without foil.



(b) With foil 1.



(c) With foil 2.

Figure 16: Energy spectra measured with Lohengrin set to $A/Q/E = 89/24/94$ both the measured spectrum (blue) and the Gaussian curve-fit (red) are shown. The masses $A = 89$ and $A = 100$ are visible without foil (a), foil 2 (c) causes separation of the $A = 89$ peak into $Z = 36$ and $Z = 35$. In the spectrum from foil 1 (b) it was not possible to fit two peaks, even if there is a hint of $Z = 35$.

6.4. Trapezoidal Filter Tuning & Energy Dependence

To compare the tested trapezoidal filter settings the best point of comparison between the two series without foil is the runs at $A/Q/E = 100/20/100$. This setting on Lohengrin was measured

in both series and therefore allows for a direct comparison. Figure 17 shows the two spectra alongside each other with *no_foil_1* to the left (fig. 17a) and *no_foil_2* to the right (fig. 17b). Note here that the number of counts was much lower for *no_foil_2*, it was especially low for the $E = 105$ MeV peak. The lower number of counts is due to a shorter measurement time, the count rates were the same.

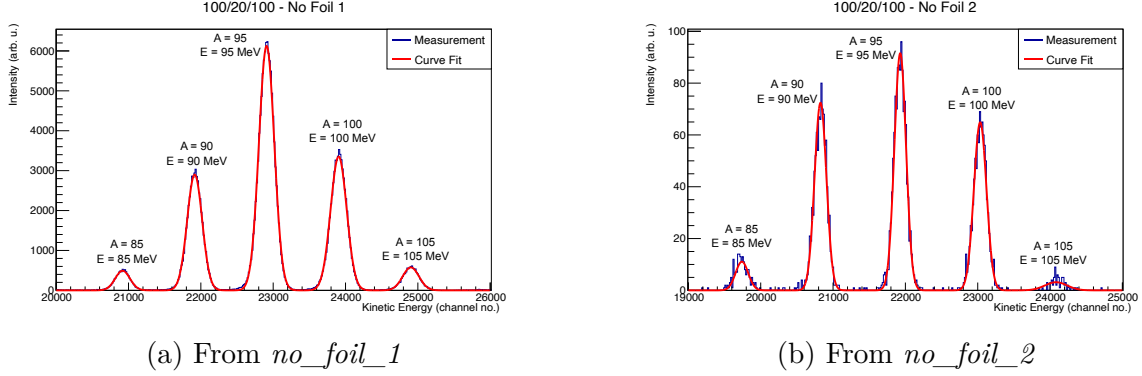


Figure 17: The figure shows an energy spectrum with Lohengrin set to $A/Q/E = 100/20/100$ from series *no_foil_1* (a) and *no_foil_2* (b). In both spectra the masses $A = 85, 90, 95, 100$ and 105 are visible at the energies $E = 85, 90, 95, 100$ and 105 MeV.

The energy resolution in terms of (E_{FWHM}/E) can be seen in table 5. From the table it is clear that the peaks are much narrower for *no_foil_2* than *no_foil_1*, around 40% lower for $E = 90, 95$ and 100 MeV.

Table 5: The table compares the resolution (E_{FWHM}/E) without foil for the two tested configurations of the trapezoidal filter for each peak visible at 100/20/100.

| Energy (MeV) | No Foil 1 $\left(\frac{E_{\text{FWHM}}}{E}\right)$ | No Foil 2 $\left(\frac{E_{\text{FWHM}}}{E}\right)$ |
|--------------|--|--|
| 85 | 1.158(1) % | 0.77(2) % |
| 90 | 1.114(4) % | 0.64(1) % |
| 95 | 1.090(3) % | 0.63(1) % |
| 100 | 1.086(3) % | 0.62(2) % |
| 105 | 1.077(1) % | 1.06(2) % |

It is also possible to plot the resolution as a function of energy for the measurement at 100/20/100 because it provides multiple high yield masses in the same spectrum. This produces figure 18, which shows the resolution as approximately constant with a slight broadening for $E = 85$ MeV, and significant broadening for the $E = 105$ MeV peak for *no_foil_2*.

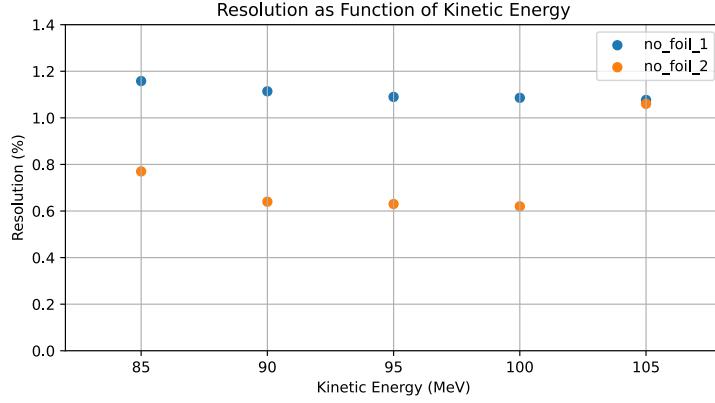


Figure 18: Resolution in terms of E_{FWHM}/E as function of energy for the five peaks visible using 100/20/100 without foil.

6.5. Foil Performance

Regarding the performance of the foils, it can be qualitatively noted from the spectra shown in section 6.3. that the individual peaks appear in the measurements with foils. This was quantified by comparing FWHM for equal settings and mass, A , with foil and without, see table 6. Table 7 shows the result for the peaks where nuclear charges could be separated using the first foil, alongside the resolution in terms of $Z/\Delta Z$. Similarly, table 8 shows the resolution for the second foil.

Table 6: Table comparing FWHM without foil and with each of the two foils for equal settings on Lohengrin ($A/Q/E$) and mass A .

| Setting | A | No Foil 2 E_{FWHM} (MeV) | Foil 1 E_{FWHM} (MeV) | Foil 2 E_{FWHM} (MeV) |
|----------|-----|-----------------------------------|--------------------------------|--------------------------------|
| 86/19/94 | 95 | 1.03(1) | 1.39(1) | 2.62(4) |
| 86/24/94 | 86 | 0.98(1) | - | 2.96(9) |
| 89/24/94 | 89 | 0.958(6) | - | 2.27(3) |
| 92/20/94 | 92 | 0.959(4) | 1.35(4) | - |
| 99/22/94 | 99 | 0.975(6) | 1.41(2) | - |

Table 7: The table shows estimated nuclear charge resolution with the first foil for a number of different settings on Lohengrin. Listed in the table is the mass A , compared nuclear charges Z_1 and Z_2 , $\delta E/E_{\text{FWHM}}$ and nuclear charge resolution $Z/\Delta Z$.

| Setting | A | Z_1 | Z_2 | $\delta E/E_{\text{FWHM}}$ | $Z/\Delta Z$ |
|----------|-----|-------|-------|----------------------------|--------------|
| 86/19/94 | 95 | 38 | 39 | 1.09(5) | 42 |
| 92/20/94 | 92 | 36 | 37 | 1.081(3) | 40 |
| 92/20/94 | 92 | 37 | 38 | 1.076(3) | 41 |
| 99/22/94 | 99 | 39 | 40 | 1.027(4) | 41 |

Table 8: The table shows estimated nuclear charge resolution with the second foil for a number of different settings on Lohengrin. Listed in the table is the mass A , compared nuclear charges Z_1 and Z_2 , $\delta E/E_{\text{FWHM}}$ and nuclear charge resolution $Z/\Delta Z$.

| Setting | A | Z_1 | Z_2 | $\delta E/E_{\text{FWHM}}$ | $Z/\Delta Z$ |
|----------|-----|-------|-------|----------------------------|--------------|
| 86/19/94 | 95 | 38 | 39 | 1.20(3) | 46 |
| 86/24/94 | 86 | 34 | 35 | 1.57(4) | 47 |
| 89/24/94 | 89 | 35 | 36 | 1.52(7) | 55 |

A final comparison which can be made is using the measurements on 86/19/94 and the $A = 95$ peak. Separation was visible for both foils here, therefore it is an excellent point of comparison for energy losses. Table 9 shows the energy loss computed as the difference between energy measured with and without foil for each Z and foil. From the table it is visible that both the energy loss and the separation is higher for the second foil. The table also shows the energy separation δE between the two nuclear charges.

Table 9: The table shows measured energy loss E_{loss} and separation δE between $Z = 38$, $Z = 39$ and $A = 95$ with Lohengrin set to 86/19/94 after adding the two foils.

| E_{loss} (MeV) | $Z = 38$ | $Z = 39$ | δE |
|-------------------------|----------|----------|------------|
| Foil 1 | 45.3(6) | 46.8(6) | 1.5(8) |
| Foil 2 | 58.1(9) | 61.6(9) | 3.5(13) |

7. Discussion

7.1. Gain Correction Issues

The calibration procedure worked incredibly well for the measurements without foil and was expected to work just as well for the measurements with foil. The expectation being that the spots in the ΔE - E histogram should go from slanted to straight, like what is seen in figure 9. For the measurements with foil however, the slant rather appears amplified, see figure 11. There are no plausible scenarios in which the foil itself could have caused this slant, so the issue must be elsewhere.

The settings on the trapezoidal filter, as shown in table 1, are very similar between *no_foil_2* and the measurements with foil. The rise time was increased slightly as this was found to improve the resolution somewhat, however, it is hard to imagine that this would have caused the slant in the ΔE - E plots observed for the measurements with foil. Especially when the measurements from the signal generator gave an almost identical difference in gain.

A more plausible explanation is some sort of noise in the measurement setup. Some issues with electronic noise were experienced earlier in the measurement cycle. It is possible that these returned when some component was moved or bumped during the installation of the foils. An oscilloscope was used to verify that the signal from the preamplifiers was clean, however it is possible that human error caused something to be missed at some stage. Noise seems like the most plausible explanation, because of the direction of the tilt in figure 11. Additional noise on the ΔE channel would manifest as a tilt in the same manner because the noise would affect both ΔE and the total kinetic energy $E = \Delta E + E_r$, thus introducing a tilt.

Because the total kinetic energy is the projection of the ΔE - E histogram onto the x-axis, this slant will unfortunately have negatively impacted the energy resolution. When looking at the resolution results with foil this needs to be kept in mind, the attainable resolution with the foils should be higher than what was measured here without this disturbance.

As a preventative measure for the final measurement, the pulse generator could be left connected during the measurement but set to a gain which does not interfere with the energies measured. This would produce a peak of known width in the spectrum, which can be used in the live-view to detect if electronic noise has appeared. Had this been done for this test measurement it also would have been possible to quantify the amount of noise present by measuring the broadening of the peak from signal generator.

7.2. Resolution without Foil

The resolution without foil appears to be quite high. There were concerning signs when looking at the live-view during the measurement, however, this was without gain correction. After performing the gain correction, the resolution appears to be quite good and not too far away from similar measurement setups. A previous study by Quade et. al. found an FWHM of 570 keV at 89 MeV (mass 89), corresponding to an $E_{\text{FWHM}}/E = 0.64\%$. This is the same as was achieved here at 90 MeV (mass 90), see table 5, after tuning the trapezoidal filter settings. This appears to be a very good result, and there does not appear to be any issues with identifying mass peaks.

Regarding the resolution as a function of energy, figure 18, it does appear that E_{FWHM}/E is approximately constant if the lowest count peaks are excluded. In particular $E = 85$ and $E = 105$ MeV. Because of the low count rate for these peaks their statistical uncertainty, $\sigma_{\text{statistical}}$ in equation (2), will be much greater. This is not an effect of the IC, but rather an effect of the limited measurement time and quite low yields for those particular combinations of energy, mass and charge state.

It is clear from the improvement in resolution that tuning the trapezoidal filter is absolutely crucial for the resolution. Excluding the low count peaks again, a reduction in peak width of about 40% is visible in table 5. It is not possible to determine after the fact if it would be possible to further improve the resolution with even more tuning. However, given the large improvement it would likely be beneficial for the real measurement to spend some additional time on tuning.

In this test the tuning of the trapezoidal filter was done without foils, but the settings used on the filter will affect the measurements with foil just as much. It might be even more important when the foils are used because of the reduction in resolution they cause.

7.3. Isotope Identification

The foils enabled the identification of nuclear charges in several spectra, and the identification procedure seems to be self-consistent. There is some uncertainty inherent to comparing the relative height to the relative yields, because fission products with the same nuclear charge can be produced in a wide range of charge states. Therefore relative yields can deviate quite significantly from the relative peak heights, which they do, as seen in table 3 and 4. Nevertheless, the identification was quite unambiguous once the higher energy loss, and therefore lower measured kinetic energy, of higher nuclear charges was taken into account.

The inability to obtain a fit to what appears to be visible separation in some cases, such as figure 16b with foil 1, is explained using equation (3). The quantity $\sigma_{\text{statistical}}$ corresponds to the statistical uncertainty, which is related to the number of counts per peak. For some low-yield nuclides this term will be very large in comparison to neighboring higher yield nuclides, and due to the common peak width fit this can make it impossible to obtain a good fit. The statistical uncertainty would be lowered by measuring for longer, which will be possible during the yield measurement. Due to the limited beamtime for this test it was not possible here. For this reason, the inability to fit these should not be directly attributed to the foils.

7.4. Foil Performance

In section 6.5. it was observed that the foils reduce the resolution markedly compared to the measurements without foil. In absolute terms the FWHM appears to increase by about 0.4 MeV for the first foil and 1.5 MeV for the second, see table 6. The increased broadening of the second foil compared to the first seems reasonable when looking at the energy loss in the foil, see table 9, the losses for foil 2 are about 15 MeV higher with 2 MeV larger separation between the neighboring charges, indicating that foil 2 is thicker. By these numbers foil 2 looks like a better choice as the increased separation should outweigh the increased peak width, which is confirmed by the $Z/\Delta Z$ resolution which is higher for foil 2 than foil 1, see table 7 and 8 respectively.

Looking closer at the spectra from foil 2, in particular figure 14c. It appears that the energy resolution is so poor with foil 2 that different the masses $A = 86$ and $A = 95$ have almost merged, this is not captured in the numbers above but could make it difficult to identify nuclear charges. The narrower peaks obtained with foil 1 provide better mass separation at the same settings as can be seen in figure 14b.

A discrepancy which should be noted is the extraordinarily high nuclear charge resolution $\frac{Z}{\Delta Z} = 55$ observed for 89/24/94 at $Z = 36$ (table 8) with foil 2. There is no physical reason for such a dramatic difference in resolution between $Z = 36$ and the others. The energy separation appears to be similar to the other peaks, however, the peak width is very narrow as per table 6. It does not look like it is overfitting in figure 16c, so it is a little unclear why the peak is so narrow. Given that two out of three masses indicate a lower resolution this seems to be an outlier.

Turning to literature, there have been previous measurements using a Parylene C foil stack which can be used as a comparison, such as one performed by Quade et al. [12]. Quade used a similar two-segment IC at Lohengrin and obtained a resolution of $Z/\Delta Z = 58$ for $Z = 39$, which is significantly higher than the $Z/\Delta Z = 42$ and $Z/(\Delta Z) = 46$ obtained here for foil 1 and foil 2, respectively (see tables 7 and 8). The results are more in line with an older result by Clerc et al. using carbon foils which achieved a lower resolution of $Z/\Delta Z = 45$ for $Z=40$ [17].

The two most likely explanations for the lower resolution compared to the literature values using Parylene C are imperfections in the foil and the electronic noise discussed in section 7.1. The noise definitely plays a role, but it is difficult to quantify how big a role it plays as there are no measurements without foil which show the same effect. Without a reliable way to quantify the noise it is unfortunately not possible to determine how much the foils contribute to broadening.

Despite the lower resolution compared to previous results the resolution obtained here should theoretically be sufficient for isotopic yield identification at the mass range targeted. The energy

separation between neighboring charges around $Z = 30$ should be greater than it is around $Z = 40$ where nuclear charge separation was observed here. Both foils should in theory be able to reach the required nuclear charge separation, however, given how low the energy resolution of the second foil is the first foil seems like a better choice. Even based on their worst $Z/\Delta Z$ of 40 (for $Z = 40$) and 46 (for $Z = 37$), both foils exceed the target $Z/\Delta Z = 35$ and should make separation possible in the target mass range.

8. Conclusion & Outlook

In conclusion it was determined that the ionization chamber itself performed similarly to what has been observed in literature with similar setups. [12] The chamber achieved a FWHM of 0.640(2) MeV at 90 MeV (mass $A = 90$).

The foils achieved $Z/\Delta Z = 40$ for $Z = 37$ and $Z/\Delta Z = 46$ for $Z = 39$, respectively. This exceeds the target set out in the introduction of one FWHM of separation for $Z < 35$. However, the measured resolution with the foils is lower than what has been observed with similar setups. A part of this is attributable to electronic noise. As it was not possible to quantify the electronic noise it cannot be ruled out that the foils themselves contributed as well. Despite these issues both foils should be usable for the final measurement, but because of the poor energy resolution of the second the first foil appears to be a better choice.

The next steps will be to make a final decision regarding whether to move forward with foil 1 or to acquire a new foil. This will be based on balancing the potential upside from increased resolution against the cost of a new foil. Despite the foils tested reaching the performance target set out here, new foils could potentially provide even higher resolution. Previous measurements with Parylene C have achieved better results, as was mentioned above.

Once this decision is made the setup is ready for measuring the higher mass region of the target range. However, it is likely that the lower mass range will have too low yields to be measured without using the RED magnet. When the RED magnet is active the beam will become strongly focused. Were the foil to be used alongside the magnet the fission products would enter the foil at a wide range of angles, traversing different distances through the foil and drastically reducing energy resolution. It is likely that a different technique would need to be used in this case.

A plausible alternative would be to use the allow the first segment of the IC to operate as a gaseous absorber. By measuring the ions time of flight in each segment of the IC the incident angle of the fission products can be computed and corrected for. This likely would not provide enough resolution to identify nuclear charges at the higher masses targeted (around $A = 80$), but is hypothesized to be enough for the lower mass range (around $A = 70$). However, this would need to be verified in a future test.

Acknowledgements

First of all, I would like to thank Ulli Koester and Jean Michel Daugas for their invaluable help in performing the measurements back in June 2024, their insights into the performance characteristics of Lohengrin have been invaluable. Secondly, I would like to thank my excellent supervisor Ali Al-Adili for his continual support and interest in the results from this work.

References

- [1] Japan Atomic Energy Agency, “Graph of Fission Product Yields.” Accessed: Nov. 14, 2024. [Online]. Available: <https://www.ndc.jaea.go.jp/cgi-bin/FPYfig?iso=nU233&eng=e1>
- [2] IAEA, “Thorium fuel cycle — Potential benefits and challenges.” [Online]. Available: https://www-pub.iaea.org/MTCD/Publications/PDF/TE_1450_web.pdf
- [3] J. Sida, P. Armbruster, M. Bernas, J. Bocquet, R. Brissot, and H. Faust, “Mass, charge, and energy distributions in very asymmetric thermal fission of ^{235}U ,” *Nuclear Physics A*, vol. 502, pp. 233–242, 1989, doi: [https://doi.org/10.1016/0375-9474\(89\)90664-7](https://doi.org/10.1016/0375-9474(89)90664-7).
- [4] D. Rochman *et al.*, “Super-asymmetric fission in the ^{245}Cm (nth, f) reaction at the Lohengrin fission-fragment mass separator,” *Nuclear Physics A*, vol. 735, no. 1–2, pp. 3–20, 2004.
- [5] P. Armbruster *et al.*, “The recoil separator Lohengrin: Performance and special features for experiments,” *Nuclear Instruments and Methods*, vol. 139, pp. 213–222, 1976, doi: [https://doi.org/10.1016/0029-554X\(76\)90677-7](https://doi.org/10.1016/0029-554X(76)90677-7).
- [6] J. S. Lilley, *Nuclear physics : principles and applications*. in The Manchester physics series. Chichester: Wiley, 2001.
- [7] A. Belyaev *et al.*, “Some peculiarities in ionic charge distributions of ^{241}Pu (nth, f)-fission products,” *Nuclear Instruments and Methods in Physics Research Section B: Beam Interactions with Materials and Atoms*, vol. 43, no. 1, pp. 5–8, 1989, doi: [https://doi.org/10.1016/0168-583X\(89\)90070-0](https://doi.org/10.1016/0168-583X(89)90070-0).
- [8] J. Ziegler, “SRIM—The Stopping and Range of Ions in Matter.” [Online]. Available: <http://www.srim.org/>
- [9] S. Julien-Laferrière *et al.*, “Fission fragments observables measured at the LOHENGRIN spectrometer,” *EPJ Web of Conferences*, vol. 239, p. 5017, 2020, doi: [10.1051/epjconf/202023905017](https://doi.org/10.1051/epjconf/202023905017).
- [10] F. Martin *et al.*, “Measurements of the mass and isotopic yields of the ^{233}U (nth, f) reaction at the Lohengrin spectrometer,” in *2011 2nd International Conference on Advancements in Nuclear Instrumentation, Measurement Methods and their Applications*, 2011, pp. 1–7. doi: [10.1109/ANIMMA.2011.6172920](https://doi.org/10.1109/ANIMMA.2011.6172920).
- [11] D. Rochman *et al.*, “Isotopic yields from the reaction ^{245}Cm (nth,f) at the Lohengrin mass separator,” *Nuclear Physics A*, vol. 710, no. 1, pp. 3–28, 2002, doi: [https://doi.org/10.1016/S0375-9474\(02\)01026-6](https://doi.org/10.1016/S0375-9474(02)01026-6).
- [12] U. Quade, K. Rudolph, and G. Siegert, “A high resolution ionisation chamber tested with fission products of ^{235}U ,” *Nuclear Instruments and Methods*, vol. 164, no. 3, pp. 435–436, 1979, doi: [https://doi.org/10.1016/0029-554X\(79\)90075-2](https://doi.org/10.1016/0029-554X(79)90075-2).
- [13] W. Schneider, “Anwendung von flugzeitmethoden zur teilchenidentifizierung,” in *GSI-Report*, 1972, pp. 22–39.
- [14] R. Brun *et al.*, “root-project/root: v6.18/02.” [Online]. Available: <https://doi.org/10.5281/zenodo.3895860>

- [15] C. Nordling and J. Österman, *Physics handbook : for science and engineering*, Ninth edition. Lund: Studentlitteratur, 2020.
- [16] K.-H. Schmidt, B. Jurado, C. Amouroux, and C. Schmitt, “General Description of Fission Observables: GEF Model Code,” *Nuclear Data Sheets*, vol. 131, pp. 107–221, 2016, doi: <https://doi.org/10.1016/j.nds.2015.12.009>.
- [17] H.-G. Clerc *et al.*, “Separation of isobaric elements by the energy-loss dispersion in carbon absorber foils,” *Nuclear Instruments and Methods*, vol. 124, no. 2, pp. 607–608, 1975, doi: [https://doi.org/10.1016/0029-554X\(75\)90619-9](https://doi.org/10.1016/0029-554X(75)90619-9).